Experimental and Computational Study of the Structure and Electrochemical Properties of $Li_xM_2(PO_4)_3$ Compounds with the Monoclinic and Rhombohedral Structure

D. Morgan,*[,†,‡] G. Ceder,[†,‡] M.Y. Saïdi,[§] J. Barker,[§] J. Swoyer,[§] H. Huang,[§] and G. Adamson[§]

Computational Modeling Consultants, Inc., 24 Manor Avenue, Wellesley, Massachusetts, 02482, Massachusetts Institute of Technology, 77 Massachusetts Avenue, Cambridge, Massachusetts, 02139, and Valence Technology, Inc., 301 Conestoga Way, Henderson, Nevada 89015

Received April 26, 2002. Revised Manuscript Received July 24, 2002

This paper presents a combined computational and experimental study of the structural and electrochemical properties of monoclinic and rhombohedral $Li_xM_2(PO_4)_3$ (with a focus on M = V). The preferred sites for dilute Li occupation and stable Li ordered phases are identified. Features of the voltage curve are understood as emerging from site energetics, Li ordering, and redox couples. These features are found to be largely independent of alloying and a simple additive model is proposed to analyze the voltage curve for any cation substitution in the monoclinic structure. The model is shown to be very useful for understanding experimental results for a number of substituted compounds. Voltages for most important cations are calculated from first principles and can be combined with the simple model to predict voltage curves for new alloyed monoclinic systems.

1. Introduction

Phosphates form a class of potentially very interesting positive electrode materials for rechargeable Li batteries. The operation of a Li battery requires that Li ions have the ability to be inserted and removed from the structure of the positive electrode oxide as the battery is charged or discharged. Many phosphates form structures similar to that of the NASICON fast Na conductor.[1] In this structure SiO_4 groups link metal−oxygen octahedra into a three-dimensional network. Considerable open space exists in this network, which allows for easy conduction of alkali ions such as Na and Li. Phosphates have higher electronic conductivity than silicates and hence are more appropriate for electrode materials. While many Li-insertion electrodes, such as $LiCoO_2$ and $LiNiO_2$, suffer from poor stability in the charged state (where they are highly oxidized), phosphates are remarkably stable, even for changes in alkali-to-metal ratios larger than 1. This has offered the prospect of inexpensive, safe, and stable positive electrode materials.

Some of the first intercalation phosphates were investigated by Delmas and Hagenmuller and others for operation in rechargeable Na cells.[2−5] They characterized the structure of many of the $Na_3M_2(PO_4)_3$ phosphates (with M = Ti, V, Cr, and Fe) as being similar to the rhombohedral NASICON structure with space group *R*3*c*. These materials exist in a rhombohedral and monoclinic NASICON-like structure, which differ by the way in which the metal octahedra and phosphate tetrahedra are organized. Despite the low electrical conductivity of the host material, Na and Li could be reversibly cycled by insertion into $Na_1Ti_2(PO_4)_3$ and $Li_1Ti_2(PO_4)_3$, respectively.[6] More recently, reversible cycling of 1−2 Li has been demonstrated in $Li_{3+x}Fe_2(PO_4)_3$ and $Li_xFe_2(SO_4)_3$[7,8] and $Li_3V_2(PO_4)_3$.[9] It was believed that in $Li_3V_2(PO_4)_3$ only two lithiums could be cycled reversibly until recently when Saidi et al.[10] and Huang et al.[11] demonstrated extraction of the third Li from $Li_3V_2(PO_4)_3$. The reversible cycling of all Li from $Li_3V_2(PO_4)_3$ would correspond to a theoretical capacity of 197 mA·h/g. Considering the very good stability of these materials and the voltage range of operation, this performance suggests these compounds could make commercially useful positive electrode materials.

* To whom correspondence should be addressed.
† Computational Modeling Consultants.
‡ Massachusetts Institute of Technology.
§ Valence Technology, Inc.

(1) Goodenough, J. B.; Hong, H. Y. P.; Kafalas, J. A. *Mater. Res. Bull.* **1976**, *11*, 203.
(2) Delmas, C.; Cherkaoui, F.; Nadiri, A.; Hagenmuller, P. *Mater. Res. Bull.* **1987**, *22*, 631.
(3) Delmas, C.; Cherkaoui, F.; Hagenmuller, P. *Mater. Res. Bull.* **1986**, *21*, 469.
(4) Beltran Porter, D.; Olazcuaga, R.; Delmas, C.; Cherkaoui, F.; Brochu, R.; Le Flem, G. *Rev. Chim. Mineral.* **1980**, *17*, 458.
(5) Abello, L.; Chhor, K.; Barj, M.; Pommier, C.; Delmas, C. *J. Mater. Sci.* **1989**, *24*, 3380.
(6) Delmas, C.; Nadiri, A.; Soubeyroux, J. L. *Solid State Ionics* **1988**, *28−30*, 419.
(7) Padhi, A. K.; Nanjundaswamy, K. S.; Masquelier, C.; Goodenough, J. B. *J. Electrochem. Soc.* **1997**, *144*, 2581.
(8) Nanjundaswamy, K. S.; Padhi, A. K.; Goodenough, J. B.; Okada, S.; Ohtsuka, H.; Arai, H.; Yamaki, J. *Solid State Ionics* **1996**, *92*, 1.
(9) Barker, J.; Saïdi, M. Y. U.S. Patent 5,871,866, 1999.
(10) Saïdi, M. Y.; Barker, J.; Huang, H.; Swoyer, J. L.; Adamson, G. *Electrochem. Solid State Lett.* **2002**, *5*, A149.
(11) Huang, H.; Yin, S. C.; Kerr, T.; Nazar, L. F. *Adv. Mat.*, in press.

10.1021/cm020348o CCC: $22.00
Published on Web 10/15/2002

In this paper we use a combination of experimental and computational methods to characterize the structure and electrochemical properties of $Li_xM_2(PO_4)_3$ (with a focus on M = V) phosphates with the monoclinic and rhombohedral structure. The experimentally recorded charge and discharge curves show remarkably rich behavior. By combining experimental results with the results of first-principles computations, we are able to show how the voltage curve features can be traced back to the crystallography and electronic structure. This understanding leads to a heuristic model for predicting the potential curve for a variety of metal-substituted phosphates.

2. Background

Lithium and sodium positions in phosphates have been investigated with NMR, X-ray, and neutron diffraction. Although we primarily investigate $Li_xV_2(PO_4)_3$ in this paper, some of the experimental facts on related systems are also presented for comparison.

2.1. Rhombohedral $Na_3Fe_2(PO_4)_3$. Masquelier et al.[12] recently investigated the Na positions in rhombohedral $Na_3Fe_2(PO_4)_3$ and this reference offers a thorough review of both low- and high-temperature results. Using powder neutron diffraction, they were able to identify the expected two sites for Na, denoted M1 and M2. The M1 site is 6-fold coordinated and is fully occupied at room temperature at this composition. The M2 site is 8-fold coordinated and is 2/3 occupied at room temperature.[13] The motif of "lantern units" making up the rhombohedral structure and the M1 and M2 sites can be seen schematically in Figure 1. At low enough temperatures, the Na ions on the M2 sites order, reducing the symmetry to *C*2/*c* (space group 15).[12−14] With increasing temperature some Na ions were found to move from the M1 to the M2 sites, resulting in a distinct phase transition at 368 K.[14] At this temperature the high-temperature phase still contains long-range Na ordering. Above 418 K, the long-range Na ordering on the M2 sites disappears and the symmetry increases to the regular rhombohedral $R\bar{3}c$ (space group 167).[14]

2.2. Rhombohedral $Li_3Fe_2(PO_4)_3$. One might expect that the Li would occupy the same sites as the Na atoms. Interestingly, the compound $Li_3Fe_2(PO_4)_3$ is found to contain Li in a location distinct from Na and denoted by M3.[12] The M3 sites are mildly distorted regular tetragonal sites and in $R\bar{3}c$ they have Wyckoff position 36f. Li order in the M3 sites reduces the symmetry at room temperature to $R\bar{3}$ (space group 148). In this reduced space group the M3 sites break up into two groups, M3A and M3B, both with Wyckoff position 18e. In $Li_3Fe_2(PO_4)_3$ only the M3A sites were claimed to be occupied.[12] The M3A and M3B sites are shown in Figure 2.

2.3. Rhombohedral $Li_3V_2(PO_4)_3$ and $LiV_2(PO_4)_3$. Less direct information is known on these materials, but as the $Li_3V_2(PO_4)_3$ is believed to be isostructural to

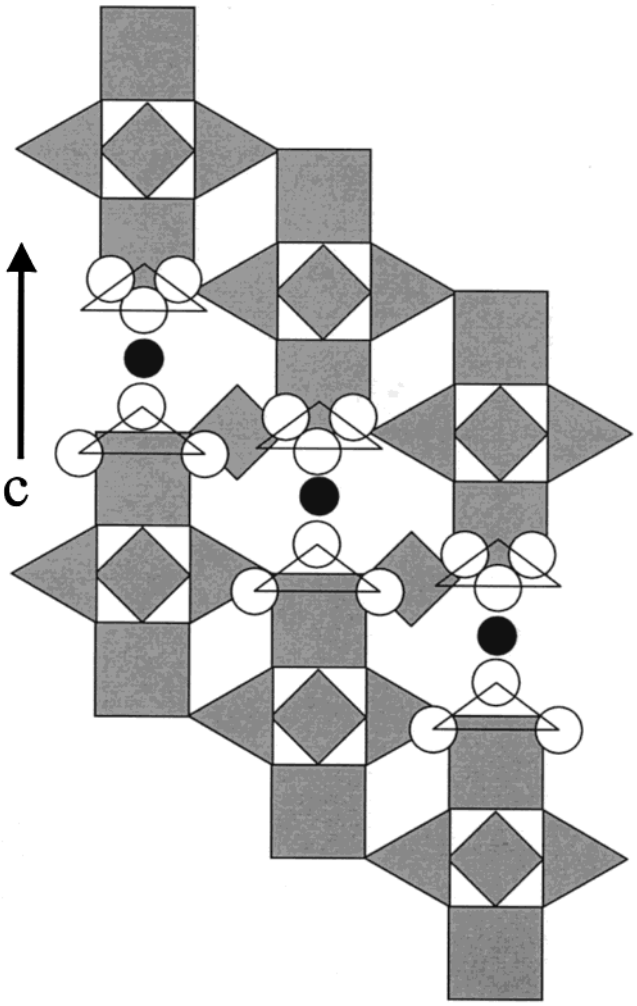

Figure 1. Schematic picture of the Rhom structure with M1 (closed circles) and M2 (open circles) positions identified.

$Li_3Fe_2(PO_4)_3$,[15] one would expect the site occupancies in the V compound to be similar to those in the Fe compound. At the $Li_1V_2(PO_4)_3$ stoichiometry, NMR results have indicated[15] that only the M1 site is occupied by Li. Indirect evidence also points to occupation of the M1 site by Li in $Li_1V_2(PO_4)_3$: Li occupation of M1 is expected to lead to a significant contraction of the *c*-axis, which is observed experimentally during electrochemical delithiation.[15]

2.4. Rhombohedral $Li_3Ti_2(PO_4)_3$ and $LiTi_2(PO_4)_3$. There is convincing evidence that in $Li_1Ti_2(PO_4)_3$ the M1 sites are occupied.[6,16] A recent investigation has indicated that in $Li_3Ti_2(PO_4)_3$ Li ions also occupy the M3-type site, but in an ordered fashion.[17]

The general trend of these results indicates that, in the rhombohedral phosphates at stoichiometry $Li_1M_2(PO_4)_3$, Li occupies the M1 site. This is somewhat surprising as it has been pointed out that this site is too large for a Li in the $Na_3Fe_2(PO_4)_3$ structure.[12] However, as will be observed in the calculations later, when Li occupies the M1 site, the structure significantly contracts around it, making the size reasonable for a

(12) Masquelier, C.; Wurm, C.; Rodriguez-Carvajal, J.; Gaubicher, J.; Nazar, L. *Chem. Mater.* **2000**, *12*, 525.
(13) de la Rochere, M.; d'Yvoire, F.; Collin, G.; Comes, R.; Boilot, J. P. in *Proceedings of the 4th International Conference on Solid State Ionics*, Grenoble, France, 1983.
(14) d'Yvoire, F.; Pintard-Screpel, M.; Bretey, E.; de la Rochere, M. in *Proceedings of the 4th International Conference on Solid State Ionics*, Grenoble, France, 1983.
(15) Gaubicher, J.; Wurm, C.; Goward, G.; Masquelier, C.; Nazar, L. *Chem. Mater.* **2000**, *12*, 3240.
(16) Paris, M.; Martin-Juarez, A.; Rojo, J.; Sanz, J. *J. Phys. Condens. Matter* 1996, *8*.
(17) Delmas, C. Private communication, 2002.

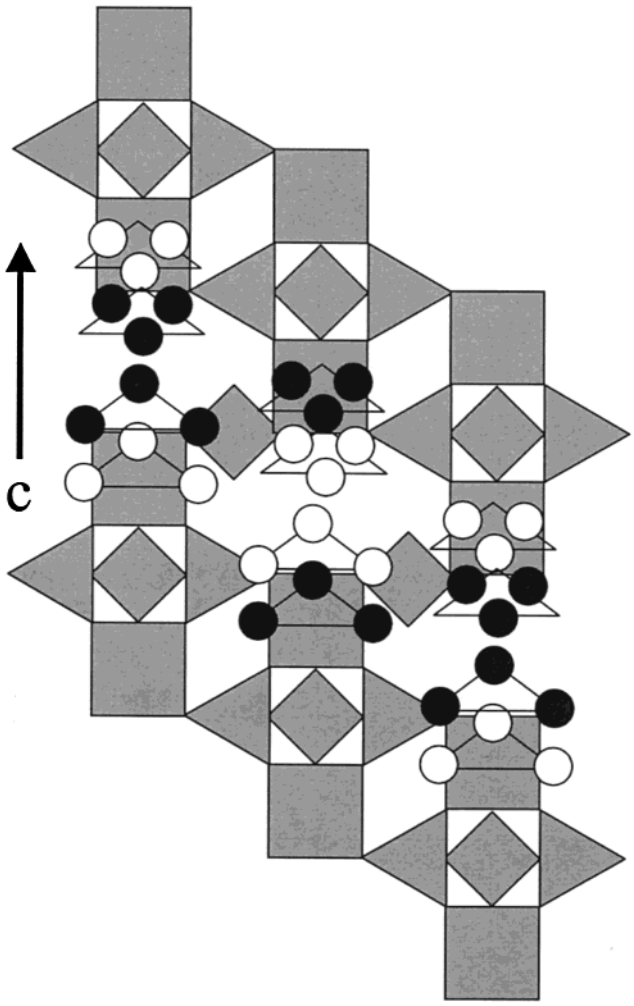

Figure 2. Schematic picture of the Rhom structure with M3A (closed circles) and M3B (open circles) positions identified.

Li^+ ion. At stoichiometry $Li_3M_2(PO_4)_3$ the phosphates investigated so far all seem to have the Li ions in positions other than M1. In all cases, occupation of M3 sites, or an ordered subset of them, have been indicated. This has some consequences for electrochemical lithium intercalation. Upon discharge of the compounds from stoichiometry $Li_1M_2(PO_4)_3$ to $Li_3M_2(PO_4)_3$ the Li ions initially present in the M1 site have to move to M3-type sites.

In section 5.3, computational methods will be used to evaluate the relative site energies in $Li_xV_2(PO_4)_3$ and $Li_xFe_2(PO_4)_3$ so as to understand the structural changes that occur upon Li intercalation and deintercalation.

2.5. Monoclinic $Li_3Fe_2(PO_4)_3$. As in the rhombohedral structure, the monoclinic structure of $A_xM_2(PO_4)_3$ contains lantern unit motifs, but in the monoclinic structure these motifs are at angles to each other, which makes the locations of the A cations more difficult to describe. A schematic picture is shown in Figure 3.

The most extensive structural information on monoclinic $Li_3Fe_2(PO_4)_3$ comes from Bykov et al.[18] Similarly to the rhombohedral (Rhom) structure, the $Li_3Fe_2(PO_4)_3$ monoclinic (Mono) structure also undergoes two phase changes upon heating. The transitions are most easily

(18) Bykov, A. B.; Chirkin, A. P.; Demyanets, L. N.; Doronin, S. N.; Genkina, E. A.; Ivanov-Shits, A. K.; Kondratyuk, I. P.; Maksimov, B. A.; Mel'nikov, O. K. *Solid State Ionics* **1990**, *38*, 31.

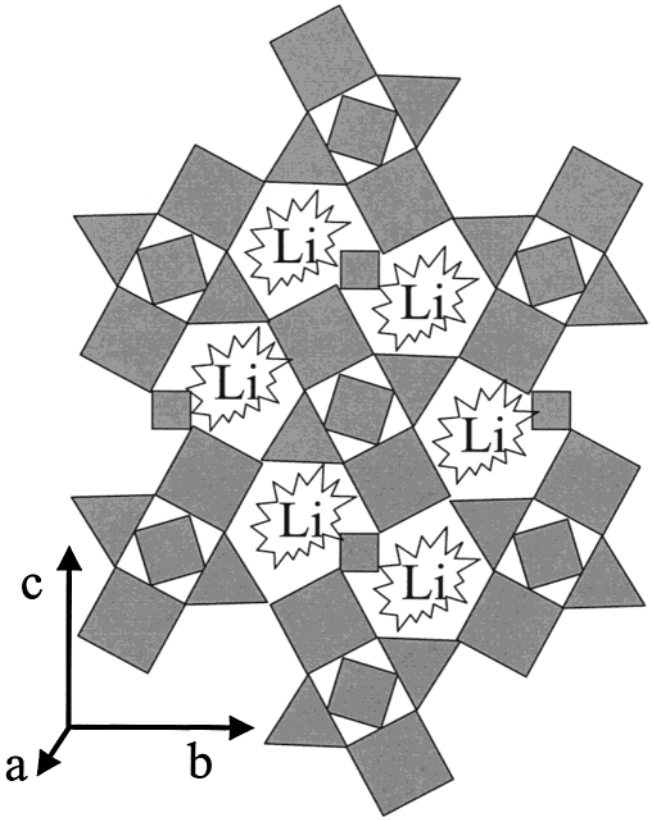

Figure 3. Schematic picture of the Mono structure with an approximate area of Li positions identified.

described by starting with the high-temperature γ phase. The γ phase has symmetry *Pbcn* (space group number 60) and the Li sit on three symmetry-distinct sites (γ1−3), with only γ1 fully occupied. All these sites are general Wykoff positions 8d and the γ1 sites are approximately regular tetrahedral sites. As the system cools, it transforms to the β phase and the symmetry is reduced to $P2_1/n$ (space group 14). This symmetry reduction splits the γ1 site into β1 and β3. Both β1 and β3 are fully occupied in the β phase. In addition, Li also fully occupies another site called β2, derived from the γ2 sites. All the sites are general Wykoff positions 4e, with the β1 and β3 sites inheriting a fairly regular tetrahedral environment from the γ1 sites. The β2 site can be described as having a distorted trigonal bipyramidal environment. Upon further cooling the system transforms to the α phase. The β and α phase are very similar and are characterized with the same $P2_1/n$ space group. All three α sites (α1−3) are general Wyckoff position 4e and fully occupied in the α phase. The three Li sites in α are almost identical to the Li sites in β, except that the α3 position is somewhat shifted from the β3 position. This makes α1 and α3 less similar than β1 and β3.

3. Experimental Methods and Results

The rhombohedral lithium vanadium phosphate compound was prepared by first making the sodium equivalent. Sodium vanadium phosphate ($Na_3V_2(PO_4)_3$) was made by mixing stoichiometric amounts of $(NH_4)_2HPO_4$, V_2O_5, and Na_2CO_3 (Alfa-Æsar, Ward Hill, MA). The mixture was first heated to 300 °C in air for 4 h to allow H_2O and NH_3 to evolve. The reagents were then re-

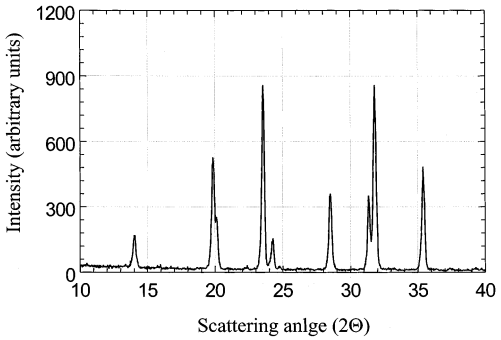

Figure 4. Experimental X-ray pattern for Rhom $Na_3V_2(PO_4)_3$.

Table 1. Comparison of Calculated and Experimental Structural Parameters for Rhombohedral Structure (All Lengths Are in Å)

$Li_1V_2(PO_4)_3$ Rhom	*a*	*c*	volume/FU	M−O avg.	P−O avg.
calculation	8.41	20.18	205.89		
experiment[15]	8.43	20.76	212.98		
$Li_3V_2(PO_4)_3$ Rhom	*a*	*c*	volume/FU	M−O avg.	P−O avg.
calculation	8.26	22.08	217.53		
experiment[15]	8.32	22.48	224.61		
$Li_3Fe_2(PO_4)_3$ Rhom	*a*	*c*	volume/FU	M−O avg.	P−O avg.
calculation	8.27	22.17	218.61	1.99	1.53
experiment[12]	8.32	22.46	224.19	2.00	1.53

ground and pelletized prior to heating in a sealed tube furnace. The sample was heated at a rate of 2 °C/min to 930 °C under a stream of pure hydrogen. The material was held for 8 h at the upper temperature and slowly cooled to room temperature prior to removal from the furnace. The initial characterization of the material was carried out using powder X-ray diffraction (XRD), using a Siemens D5000 diffractometer and Cu Kα radiation. The unit cell parameters for the rhombohedral phase were obtained from a least-squares refinement of the XRD pattern using the *hkl* indices for space group $R\bar{3}c$ and are shown in Table 1. The XRD experimental pattern is shown in Figure 4.

The resulting $Na_3V_2(PO_4)_3$ was then ion-exchanged with lithium in a solution containing a 5-fold molar excess of LiBr (Sigma-Aldrich, Milwaukee, WI) to achieve the desired $Li_3V_2(PO_4)_3$ product. The LiBr was first dissolved into deionized water at a ratio of 1 g of LiBr/100 mL of water. The solution was heated to about 50 °C while being stirred slowly with a magnetic stirrer on the hot plate. The $Na_3V_2(PO_4)_3$ was then slowly introduced into the solution and the mixture was stirred and heated overnight. The mixture was then cooled and allowed to settle. The liquid was decanted off and the resulting $Li_3V_2(PO_4)_3$ powder was washed several times with deionized water followed with vacuum filtration. The product was then dried in a vacuum oven overnight at 200 °C to remove residual moisture.

The monoclinic lithium vanadium phosphate was prepared by mixing stoichiometric amounts of $NH_4H_2PO_4$, V_2O_5, and Li_2CO_3 (Alfa-Æsar, Ward Hill, MA). The mixture was initially heated to 300 °C in air for 4 h to allow H_2O and NH_3 to evolve. The resulting product was then ground, pelletized, and heated to 850 °C under a stream of pure hydrogen for 8 h in a sealed tube furnace. Once the furnace had cooled to room temperature, the pellet was crushed and prepared for electrode processing. Equivalent monoclinic compounds, based on mixtures of V/Ti, V/Cr, and V/Al couples, were prepared in the same manner where the vanadium was partially replaced by an alternative metal oxide. $Li_3V_2(PO_4)_3$ electrodes were prepared by mixing with a conductive carbon, Super P (Erachem, Belgium), and a binder, PVDF−HFP copolymer (Kynar 2801, Alfatochem). The electrode constituents were mixed into a slurry with acetone to achieve homogeneity. The resulting slurry was coated onto a glass plate using a doctor blade. After the acetone had evaporated, the resulting electrode composition was 80:10:10 of active material, carbon, and binder, respectively. The electrode was then dried and transferred into an argon-filled glovebox for cell assembly. The electrode was cut into a $^3/_4$-in.-diameter disk and placed on top of an aluminum foil current collector. Glass fiber separator was placed between the $Li_3V_2(PO_4)_3$ positive electrode and lithium metal, pressed onto a copper current collector, as the anode. The electrolyte used consisted of a 1 M solution of $LiPF_6$ in a mixture 2:1 by weight of ethylene carbonate (EC) and dimethyl carbonate (DMC) (Grant-Ferro, Louisiana).

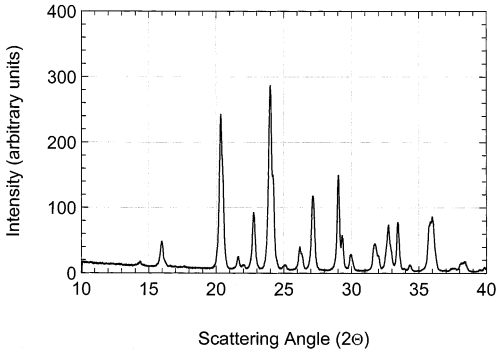

Figure 5. Experimental X-ray pattern for Mono $Li_3V_2(PO_4)_3$.

The powder purity and crystallinity were determined by powder X-ray diffraction. The X-ray diffractogram shows a highly crystalline phase with no detectable impurities, as seen in Figure 5. The initial characterization of the material was carried out using powder X-ray diffraction (XRD), using a Siemens D5000 diffractometer and Cu Kα radiation. The experimental pattern shown in Figure 5 is consistent with that previously shown by Goodenough and co-workers.[19] The unit cell parameters and atomic positions for the monoclinic phase were obtained from a least-squares refinement of the XRD pattern with space group $P121/n1$. The unit cell parameters are summarized in Table 2.

Voltage traces were collected using the electrochemical voltage spectroscopy (EVS) technique. EVS increments the voltage in small steps, taking the next step only after the current decays to a cutoff critical current density. The critical current density is chosen small enough to ensure that voltage corrections due to the cell IR drop and diffusion overvoltages are small. This technique yields accurate information regarding structural phase transformation and order/disorder phenomena.[20] This technique was also used to study similar reactions in conducting polymers.[21] The conditions

(19) Okada, S.; Arai, H.; Asukara, K.; Sakurai, Y.; Yamaki, J.; Najundaswami, K. S.; Padhi, A. K.; Masquelier, C.; Goodenough, J. B. *Prog. Batteries Battery Mater.* **1997**, *16*, 302.
(20) Thompson, A. *Phys. Rev. Lett* **1978**, *23*, 1511.

Table 2. Comparison of Calculated and Experimental Structural Parameters for Mono Structure (All Lengths Are in Å)

$Li_3V_2(PO_4)_3$ Mono	*a*	*b*	*c*	*b*	volume/FU	M−O avg.	P−O avg.
calculation	8.56	8.51	11.92	89.75	217.05	1.97	1.53
experiment[10]	8.662	8.624	12.104	90.452	226.04	NA	NA
$Li_3Fe_2(PO_4)_3$ Mono	*a*	*b*	*c*	*b*	volume/FU	M−O avg.	P−O avg.
calculation	8.54	8.60	11.85	90.65	217.73	1.99	1.53
experiment[18]	8.56	8.61	12.01	90.51	221.31	2.01	1.53

chosen for the cell cycling were voltage limits between 3.0 and 4.2 V (vs Li/Li^+), voltage step sizes of 10 mV, and critical current density $<100\ \mu A/cm^2$. These conditions were chosen so as to maintain the system close to thermodynamic equilibrium throughout the discharge/charge cycle. As such, the voltage profile should provide a close approximation to the open cell voltage (OCV)−composition relationship.

4. Computational Methods

The phosphate structures are remarkably complex and the large open spaces between the phosphate−octahedra linkages create several possible locations for the Li ions. A first-principles methodology is ideal for investigating the relative energy of Li in all these locations since, as a computational approach, it offers complete control and characterization of the system under study. The energy of Li in different positions in the structure can systematically be investigated by calculations on supercells with various Li positions. From the energy of these Li positions, the potential at which the Li is extracted can be evaluated. We demonstrate in this manuscript that this approach leads to an effective characterization of the structural rearrangements during Li cycling.

All calculations were performed in the local density approximation (LDA) to density functional theory as implemented in the Vienna Ab Initio Simulation Package (VASP).[22,23] The unit cells of the relevant structures may contain up to 80 ions, making computations on these materials particularly demanding. In some calculations we employed the generalized gradient approximation (GGA) rather than the LDA, and these cases will be noted explicitly. The nuclei and core electrons were represented with ultra-soft pseudopotentials and all structures were fully relaxed with respect to internal and external cell parameters and atomic positions, unless explicitly stated. The wavefunctions were expanded in plane waves with kinetic energy below 405 eV. Brillouin zone integration of the band structure was performed at the gamma point (Mono) or with an odd $2 \times 2 \times 2$ Monkhorst-Pac mesh (Rhom). Absolute energies for the Rhom structure were converged with respect to *k*-points to within 10 meV/FU and the absolute energies for the Mono structure were converged to within 90 meV/FU. Unfortunately, the large size of the Mono unit cell made more accurate convergence of the Mono energies impractical. However, since 90 meV/FU is the absolute error, energy differences will be converged to a significantly greater accuracy. Unless otherwise stated, the charge density was ferromagnetically spin-polarized. This is an approximation, since most oxide systems are anti-ferromagnetic. However, the large separation of the metal atoms in these materials results in little difference between the ferromagnetic and anti-ferromagnetic energies. A recent experimental study by Rousse et al.[24] on NASICON $Li_3Fe_2(PO_4)_3$ structures suggests that they have weak magnetic interactions, supporting our claim that these interactions can be ignored. We have also performed a calculation for Mono α-$Li_3Fe_2(PO_4)_3$ and found that a reasonable anti-ferromagnetic ordering is more stable than ferromagnetic ordering by only about 60 meV/FU. Because $Li_xV_2(PO_4)_3$ has a smaller moment than $Li_xFe_2(PO_4)_3$, we expect the magnetic effects in the V materials are even less important than those in Fe compounds.

Table 3. Rhom Alkali Cation Site Environments (All Data Taken from Reference 12)

system	site	Wykoff	occ.	coord.	bond lengths (Å)
α-$Na_3Fe(PO_4)_3$	M1	6b ($R\bar{3}c$)	1	6 (octahedral)	2.44−2.46
α-$Na_3Fe(PO_4)_3$	M2	18e ($R\bar{3}c$)	$^2/_3$	8	2.37−2.90
$Li_3Fe(PO_4)_3$	M3A	18f ($R\bar{3}$)	1	4 (tetragonal)	1.92−2.20

5. Computational Results

5.1. Structural Parameters. As a simple check on the validity of our calculations, we compare some structural parameters. Results for the Rhom and Mono structures are shown in Tables 1 and 2, respectively. The calculations show the usual reduction of lengths by up to a few percent associated with use of the local density approximation.[26]

5.2. Site Energies in the Rhombohedral Structure. We will focus on the M1, M2, and M3 sites, whose characteristics are briefly summarized in Table 3. The relative energies of the M1, M2, and M3 sites are determined by calculating the energy of supercells with a single Li inserted in one of these sites. The structures are fully relaxed so that no forces on the atoms remain. Our supercell contains two formula units so that the effective composition of the lithiated material is $Li_{0.5}M_2(PO_4)_3$. We believe this result to be representative of isolated Li ions since at this composition Li ions are more than 8 Å apart. The energy of M1 is set to zero as a reference. From the fact that we are treating isolated Li in a host with space group $R\bar{3}c$, it follows that the M3A and M3B sites are equivalent, and they will be referred to collectively as M3 sites. The results in Table 4 show that the M1 site is most stable for both the V and Fe compounds. In $Li_{0.5}Fe_2(PO_4)_3$, the M3 site is unstable and relaxes to M1.

(21) Barker, J. *Synth. Met* **1989**, *32*, 43.
(22) Kresse, G.; Hafner, J. *Phys. Rev. B* **1994**, *49*, 14251.
(23) Kresse, G.; Furthmüller, J. *Comput. Mater. Sci.* **1996**, *6*, 15.
(24) Rousse, G.; Rodriguez-Carvajal, J.; Wurm, C.; Masquelier, C. *Chem. Mater.* **2001**, *13*, 4527.
(25) Reiff, W. M.; Zhang, J. H.; Torardi, C. C. *J. Solid State Chem.* **1986**, *62*, 231.
(26) Van de Walle, A.; Ceder, G. *Phys. Rev. B* **1999**, *59*, 14992.

Table 4. Relative Stability of Isolated Li in Rhom M1−3 Sites

$x = 0.5$, $Li_{0.5}M_2(PO_4)_3$, E(meV/Li)	E(M1)	E(M2)	E(M3)
V	0	390	160
Fe	0	970	20 (unstable)

The calculated stability of M1 is consistent with the experimental evidence that for $x = 1$ Li tends to occupy the M1 sites in the Rhom structure (see section 2.3). The calculations indicate a surprising flexibility of the structure as the M1 site is filled. In α-$Na_3Fe_2(PO_4)_3$ the average Na−O bond length is 2.444 Å for Na in the M1 sites. Our calculations give an average Li−O bond length of only 2.106 Å for M1 Li in $LiFe_2(PO_4)_3$. It is presumably due to this exceptional flexibility that the Rhom structure can accommodate both the Na and Li in quite different size M1 cavities.

It is reasonable to expect that Li will continue to enter M1 sites until they are all filled, which occurs for $x = 1$ Li per formula unit. Note that the presence of a particularly stable Rhom phase at $x = 1$ is consistent with the fact that for some metals it is possible to form the Rhom structure at this composition directly, without the use of ion exchange.[27]

It is of some interest to confirm the experimental observation that the Li will occupy the M3 sites at $x = 3$. We have calculated the relative stability of two possible Li arrangements, one in which all the M3A sites are occupied and one in which $^2/_3$ of the M3A sites are occupied and all the M1 sites are occupied. The latter configuration is less stable by 611 meV/FU. These results suggest that at $x = 3$ the Li are much more stable depopulating the M1 sites and occupying M3 sites, in agreement with the experimental results.[6,12,15]

We know that for the fully lithiated material the M1 sites are empty so that between $x = 1$ and $x = 3$ Li ions must move from the M1 to the M3A sites. Recent experimental work has shown that $Li_xV_2(PO_4)_3$ has a two-phase region between $x = 1$ and $x = 3$ at room temperature.[28] Although we have only examined one intermediate concentration ($x = 1.5$), we did find an ordering tendency at this concentration. We tried two Li configurations at $x = 1.5$, one consisting of occupancy of all M1 sites and one M3A site and one consisting of occupancy of only M3A sites. This former Li arrangement was found to be more stable by about 228 meV/FU, suggesting that the M1 sites are still occupied at $x = 1.5$. The formation energy of the more stable structure with respect to the stable structures at $x = 1$ and $x = 3$, given by $E_{form}(x{=}1.5) = E_{Tot}(x{=}1.5) - 0.75E_{Tot}(x{=}1) - 0.25{*}E_{Tot}(x{=}3)$, is about −40 meV/FU (although an effort was made to use relatively stable Li arrangements, these results are quite uncertain because of uncertainties in the optimal Li arrangements). It should be remembered that these calculations are for $T = 0$ K. The ordering tendency is weak enough that it could be overwhelmed by thermal excitations at room temperature, and therefore the calculated result does not necessarily contradict the experimental observation.

Figure 6 shows our calculated ($T = 0$ K) and our experimentally measured (room temperature) (de)intercalation curves. The (de)intercalation curve was calculated using standard electrochemical formulas[29] and the lowest first-principles energies we obtained for Li concentrations at $x = 0$, 0.5, 1, 1.5, and 3. It should be noted that the calculated (de)intercalation curve applies to a system perfectly at equilibrium, and therefore the intercalation and deintercalation curves are identical. In the experimentally measured data there is some shift between the intercalation and deintercalation curves due to polarization. The calculated voltages have been shifted by an overall constant (1.4 V) to provide the best possible match to the experimental results. This error in the absolute voltage will be discussed in section 5.6.

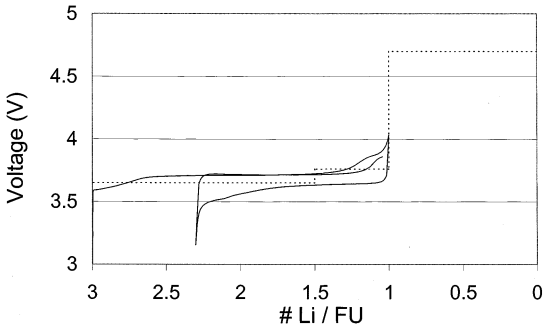

Figure 6. Comparison of room-temperature experimental (solid line) and $T = 0$ K calculated (dashed line) intercalation curve for Rhom $Li_xV_2(PO_4)_3$.

In conclusion, the experiments and calculations suggest that the Li intercalation process in the Rhom structure proceeds by *first filling the M1 sites and then depleting M1 and filling M3.* Calculations indicate that, at low temperatures, ordering could occur in the region $x = 1 \rightarrow 3$. The shift from M1 to M3A sites must be brought on either by direct Li−Li interactions or by changes in the site energies created by structural shifts caused by the presence of Li. If, at composition $Li_3V_2(PO_4)_3$, ordering would occur over the M3A and M3B sites (which we did not investigate), the energy of the $Li_3V_2(PO_4)_3$ might be lower than what we calculate and the weak ordering tendency in the region $x = 1 \rightarrow 3$ could be replaced by phase separation.

5.3. Li Sites in the Monoclinic Structure. As a starting point for our investigation of site energies in the Monoclinic (Mono) structure, we will make use of the sites in the different phases of Mono $Li_3Fe_2(PO_4)_3$. As discussed in section 2.5, there are three phases of Mono $Li_3Fe_2(PO_4)_3$, each of which have three different sets of symmetry equivalent Li sites. At first glance, we have a total of three Li positions in three different phases, giving nine site energies to consider. However, many of the sites with different names are in fact equivalent, with slight changes due to changes in symmetry. For simplicity, we will label all sites consistent with the lowest symmetry space group, $P2_1/n$. Because the low-temperature phases have lower symmetry than the high-temperature phase, each of the γ-phase sites with Wyckoff position 8e are split into two groups of Wyckoff position 4e, which will be labeled γA and γB. Thus, in space group $P2_1/n$, all the sites are α1−3, β1−3, γ1−3A, and γ1−3B, for a total of 12 sites. Fortunately, a careful examination of these sites shows

(27) Touboul, M.; Quarton, M.; Lokaj, J.; Kettmann, V. *Acta Crystallogr., Sect. C Cryst. Struct. Commun.* **1988**, *44*, 1887.

(28) Gaubicher, J.; Le Mercier, T.; Chabre, Y.; Angenault, J.; Quarton, M. *J. Electrochem. Soc.* **1999**, *146*, 4375.

(29) Aydinol, M. K.; Kohan, A. F.; Ceder, G.; Cho, K.; Joannopoulos, J. *Phys. Rev. B* **1997**, *56*, 1354.

Table 5. Site Environments of the Alkali Ion in the Monoclinic Structure (All Data Taken from Reference 18 and References Therein)

site	Wykoff	occupation	coordination	equivalences
α phase	$P12_1/n1$			
α1	4e	1	4 (regular tetrahedron)	≈γ1A
α2	4e	1	5 (distorted trigonal bipyramid)	≈γ2A
α3	4e	1	5 (distorted trigonal bipyramid)	
β phase	$P12_1/n1$			
β1	4e	1	4 (regular tetrahedron)	≈γ1A
β2	4e	1	5 (distorted trigonal bipyramid)	≈γ2A
β3	4e	1	4 (regular tetrahedron)	≈γ1B
γ phase	*Pbcn*			
γ1	8d	1	4	
γ2	8d	0.25	5	
γ3	8d	0.25	4	

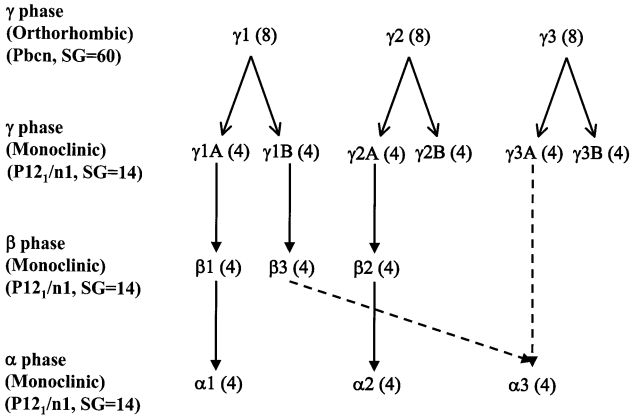

Figure 7. Correspondence among Mono Li positions for different phases. Multiplicities of each position are given in parentheses after the position label.

that many of them can be considered equivalent. The symbol ≈ will be used to denote sites that are in very similar environments. The α and β phases are very closely related and by examining the positions it is clear that α1≈β1 and α2≈β2. Again by examining the positions it can be seen that in the γ→β transition the γ1 positions are split into β1 and β3 and that half the γ2 positions become the β2 positions. We therefore can extend the approximate equivalence of positions to β1≈γ1A, β3≈γ1B, and β2≈γ2A. These equivalencies are all summarized in Figure 7.

In summary, we have determined seven candidate symmetry distinct Li positions in the $P2_1/n$ symmetry Mono structure: γ1A, γ1B, γ2A, γ2B, γ3A,γ3B, and α3. Because the monoclinic distortion away from orthorhombic tends to be fairly minor, even in the monoclinic space group $P2_1/n$, the γA and γB sites are very similar. The γA and γB are pseudo-symmetric under *Pbcn* (i.e., these sites are almost mapped onto one another by symmetry operations of *Pbcn*). If we assume that the γA and γB sites are likely to yield similar energies, then the number of distinct candidate Li positions is reduced to only 4: γ1A, γ2A, γ3A, and α3. Some basic characteristics of the Li sites, based on experimental data, are shown in Table 5.

The lowest energy Li arrangement for $Li_3Fe_2(PO_4)_3$ involves filling the α1−3 sites.[18] However, from the experimental fact that in the γ-phase the γ1 sites are fully occupied while the γ2 and γ3 sites are only $^1/_4$ occupied,[18] we can infer that the γ1 (and therefore α1) sites are likely to be the most stable. This will be verified by calculations discussed in section 5.4.1.

Li insertion into the Mono structure is more complex than the Rhom structure since there are more sites involved. To guide us in our investigation, we start with the experimental intercalation curve for $Li_xV_2(PO_4)_3$, shown in Figure 8.[10] From this curve we identify a few critical compositions: dilute ($x \approx 0$), $x = 1$, $x = 2$, and $x = 3$. We will begin by identifying the Li structures at these compositions. In some cases we will perform calculations replacing V with Fe to provide additional support for the results.

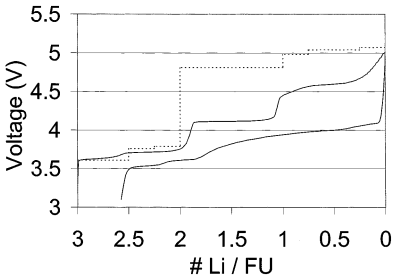

Figure 8. Comparison of room-temperature experimental (solid line) and $T = 0$ K calculated (dashed line) intercalation curve for Mono $Li_xV_2(PO_4)_3$.

Table 6. Relative Stability of Isolated Li in Candidate Mono Sites

$x = 0.25$, $Li_{0.25}M_2(PO_4)_3$, E(meV/Li)	γ1A	γ2A	γ3A	α3
V	0	230	80	110
Fe	0	170	200	280

5.4. Li Structures at Key Compositions ($x \approx 0$ (dilute), 1, 2, and 3). *5.4.1. $x \approx 0$ (Dilute).* In our calculations $V_2(PO_4)_3$ relaxed to a structure with a monoclinic angle of $\beta = 90.16°$ (an angle of 90° would correspond to an orthorhombic structure). This is consistent with the fact that $Fe_2(SO_4)_3$ and $FeTi(SO_4)_3$ are found to be monoclinic.[8] Thus, the first Li are entering a monoclinic host, albeit one which is very close to being orthorhombic. In Table 6 we show the relative energies for Li in the γ1A, γ2A, γ3A, and α3 sites as calculated by inserting Li into a supercell. Because of the finite size supercells, the concentration of Li is $x = 0.25$ Li per formula unit. However, the Li ions are more than 8 Å from their nearest neighbors and we believe this can represent an isolated Li. The results in Table 6 indicate that the γ1 position is the most stable site for both V and Fe. These stable sites are tetrahedrally coordinated (see Table 5), which we believe is the key to their high stability. While there is no experimental information concerning site occupations at low lithium concentration for these materials, our results are consistent with the experimental finding that the γ1 sites are fully occupied in the gamma phase of $Li_3Fe_2(PO_4)_3$.[18]

5.4.2. $x = 1$. At $x = 1$ we expect the Li to reside in the α sites since the α sites are filled at low temperature. However, the calculations in Table 6 demonstrate that the tetrahedral sites are the most stable. Both of these conditions can be satisfied by filling the tetrahedrally coordinated α1 sites. We have checked the Li occupation, using calculations on a single primitive unit cell containing four formula units, so that for $x = 1$ four Li need to be distributed in the cell. We have compared two Li arrangements, one with filled α1 sites (a monoclinic structure) and one with filled tetrahedral sites that were not all equivalent to α1 (orthorhombic structure). Calculations on the V compound predicted the orthorhombic structure to be about 30 meV/FU higher than the monoclinic one with filled α1 sites. Although this energy difference is too small to be definitive, it supports our belief that at $x = 1$ the material will form a monoclinic phase with occupied α1 sites.

5.4.3. $x = 2$. Given that there are two $\gamma 1$ sites per formula unit, it may be expected that at this composition Li fills all the $\gamma 1$ sites. In the case of V, we calculated the energy of a structure with filled $\gamma 1$ sites and compared it to a structure where $\gamma 1$ is empty but α1 and α3 sites are filled. We found the latter to be 260 meV/FU higher in energy (this same comparison was made in the Fe compound and the α1, α3 occupied structure was found to be 220 meV/FU higher in energy). While this is by no means an exhaustive search, this result together with the stability of the $\gamma 1$ site at low Li content makes it likely that in $Li_2M_2(PO_4)_3$ all the $\gamma 1$ sites are filled. There is some other experimental information to back up this claim. In the calculations, the structure where all the $\gamma 1$ sites are filled relaxes to orthorhombic symmetry. This is consistent with the experimental observation of Torardi and Prince who showed that $Li_2Fe_2(MoO_4)_3$ was orthorhombic. Furthermore, they have found that the Li ions were located in tetrahedrally coordinated sites,[30] which are likely the γ_1 sites. Similarly, Touboul et al. found that $Li_2Mg_2(SO_4)_3$ was orthorhombic with tetrahedrally coordinated Li.[27] It has also been shown that $Li_2Fe_2(SO_4)_3$ is orthorhombic.[8]

5.4.4. $x = 3$. Experiments show that $Li_3Fe_2(PO_4)_3$ forms the monoclinic α phase, with Li occupying the α1, α2, and α3 sites.[18] For the V material we calculated the energy of this $Li_3Fe_2(PO_4)_3$ structure as well as one where the $\gamma 1$ sites were totally filled and the $\gamma 2$ and $\gamma 3$ sites were partially filled (analogous to the high-temperature γ phase[18]). The latter structure was found to be less stable by about 140 meV/FU. However, minimal effort was made to find the optimal arrangement for Li in the $\gamma 2$ and $\gamma 3$ sites, so it is possible that more stable structures exist. These results suggest that, consistent with experiments on the Fe compounds, the V compounds are most stable in the α phase.

In summary, examining these key stoichiometries suggests that intercalation in the V compound occurs first into α1 ($\approx \gamma$1A) sites. When x reaches 1, these sites are all filled, creating a monoclinic structure. Further intercalation proceeds by filling the rest of the stable $\gamma 1$ sites up to $x = 2$. The structure at $x = 2$, with filled $\gamma 1$ sites, is orthorhombic. Inserting more Li causes some rearrangements, leading to filled α1−3 sites and a monoclinic structure by $x = 3$.

5.4.5. Intermediate Compositions and Possible Ordering. Up until this point, we have focused on a few ordered compositions of $Li_xV_2(PO_4)_3$. It is possible to use fairly elaborate techniques to investigate possible ordering for all compositions and construct the Li-vacancy phase diagram,[31] but this would be very difficult in a system of this complexity. At several intermediate compositions we have constructed structures and calculated their energy. In addition to $x = 1$, 2 we find at least some ordering tendency at $x = 0.25$, 0.75, 2.25, and 2.5, though the ordering energies are often quite weak (20−50 meV/FU) so they could easily be smoothed out in a finite-temperature voltage curve.

The ordered phase at $x = 2.5$ shows the strongest ordering of the intermediate compositions and is of particular interest since it is clearly seen experimentally. It is not immediately obvious how to guess at the $x = 2.5$ Li arrangement since it is halfway between the orthorhombic structure with filled $\gamma 1$ sites ($x = 2$) and the monoclinic α phase, where the α1−3 sites are occupied ($x = 3$). We performed calculations on the V compound that involved adding Li to the $x = 2$ structure and ones that involved removing Li from the $x = 3$ structure. We found that the Li arrangements formed by adding Li to the $x = 2$ structure were the most stable, so we conclude that the $x = 2.5$ structure still has all the $\gamma 1$ sites filled, with additional Li occupying the $\gamma 2$ and/or $\gamma 3$ sites. The exact arrangement of the Li was not determined.

5.5. Open-Circuit Voltage for the Monoclinic Structure. *5.5.1. $Li_xV_2(PO_4)_3$.* Figure 8 shows the calculated ($T = 0$ K) and experimentally measured (room temperature)[10] (de)intercalation curves for Mono $Li_xV_2(PO_4)_3$. The calculated voltages have been shifted by an overall constant (+1.75 V) to match the experimental value at $x = 3$ (see section 5.6 for a discussion of the voltage shift). The experimental results have been scaled so that the total removed capacity corresponds to three Li. We will focus our comparison on the charging curve since the discharging curve has some unusual features which will be discussed at the end of this section. The main features of the experimental charging curve are the steps at $x = 2.5$, 2, and 1. We can now use the calculations to identify the origins of these main features in the experimental charging curve. The step at $x = 2.5$ corresponds to the presence of an ordered Li phase. At $x = 2$ a step occurs because one must start removing Li ions from the stable tetrahedral $\gamma 1$ sites, instead of the nontetrahedral ones. This step is significantly larger (∼0.4 V experimentally and ∼1 V from calculation) than one would expect from the site energies in Table 6, signifying considerable Li−Li interactions. The step at $x = 1$ is different in origin and due to the fact that one switches from the $V^{3+/4+}$ redox couple to the $V^{4+/5+}$.

The calculated voltage step at $x = 2$ is about 2.5 times larger than the experimentally measured value. This discrepancy could be due to the electronic structure method we used or because we might not have used the lowest energy structure for $Li_1V_2(PO_4)_3$. Finding a lower

(30) Torardi, C. C.; Prince, E. *Mater. Res. Bull.* **1986**, *21*, 719.

(31) Ceer, G.; Van der Ven, A. *Electrochim. Acta* **1999**, *45*, 131.

energy state for $Li_1V_2(PO_4)_3$ would also increase the difference of the average voltage for the $V^{4+/5+}$ and $V^{3+/4+}$ redox couples and bring it into closer agreement with experiment. It is possible that at least some V ions move to more stable nonoctahedral environments as they become oxidized to +4 or +5. It is well-known that V^{5+} is often found in distorted octahedral or nonoctahedral sites (e.g., in V_2O_5). In addition, our experiments on V systems cycled in the range $x = 1-3$ often yield yellow coloration at $x = 1$, which is evidence of V^{5+}.

This presence of V^{5+} in a nominally V^{4+} average charge state suggests that charge disproportionation ($2V^{4+} \rightarrow V^{3+} + V^{5+}$) may be occurring. Charge disproportionation would be facilitated by the shifting of some V (presumably the V^{5+}) to nonoctahedral sites. Finally, in the cases where the system is cycled to $x < 1$ (creating V^{5+}) the discharge looks very different from the charge, particularly for $x < 1$. This suggests that the system has undergone significant structural changes during charging. These structural changes might consist of shifting V^{5+} into nonoctahedral environments.

The above discussion has focused on comparing our calculations to the experimental charging curve, since the discharge curve looks quite different in the range $x = 0 \rightarrow 2$. We believe that during discharge from $x = 0$ there is initially a structural change that creates significantly different Li environments than those seen upon charging. The nature of this structural change has not been identified and is not presently included in the calculations. It is interesting to note that the structural transformation which occurs on cycling $x = 3 \rightarrow 0$ does not occur if the materials are cycled from $x = 3 \rightarrow 1$.

5.5.2. Doped Materials. The previous analysis allows us to understand and approximately predict the OCV curve for all materials with the monoclinic NASICON-like structure, for any chemistry on the transition metal site. The shape of the OCV curve is determined by the sum of the energy for Li^+ removal and the energy for oxidation of the transition metal(s). Li ordering and site selection will always impose features at $x = 2.5$ (≈30 mA·h/g) and $x = 2$ (≈60 mA·h/g). These are respectively due to ordering and to a switch between Li removal from nontetrahedral sites to tetrahedral sites. The latter are more stable and hence a higher potential is required to remove Li from them. Superimposed on this is the energy required to oxidize the metal. For $Li_3V_2(PO_4)_3$ V^{3+} to V^{4+} is active for removal of the first two lithium and hence the electron energy is relatively constant, clearly exposing the lithium features in the voltage curve. Charging past $x = 1$ requires oxidation of some vanadium to V^{5+}, causing an abrupt increase in voltage (even though no change occurs in the sites from which Li is removed).

Parts a−d of Figure 9 show, respectively, the voltage curves for $Li_3(VTi)(PO_4)_3$, $Li_3(VAl)(PO_4)_3$, $Li_3(VCr)(PO_4)_3$, and $Li_3(V_{1.5}Al_{0.5})(PO_4)_3$. Only the Ti^{3+}/Ti^{4+} redox couple is below that of V^{3+}/V^{4+}; hence, the Ti couple will be oxidized first. This shows up as a depression of the initial part of the charging curve (Figure 9a). Near $x = 2$ (≈60 mA·h/g) both the sites from which Li is removed and the active redox couple change. The capacity between $x = 2$ and $x = 1$ (≈60 mA·h/g to ≈120 mA·h/g) consists of removing Li from tetrahedral sites and electrons from V^{3+}, hence the similarity in voltage with

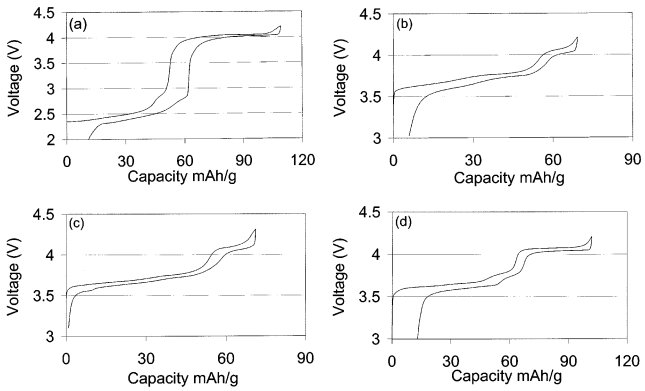

Figure 9. Experimental voltage curves for doped Mono V alloys: (a) TiV, (b) AlV, (c) CrV, and (d) $Al_{0.5}V_{1.5}$.

that of the pure $Li_3V_2(PO_4)_3$. The rapid increase in voltage near ≈50 mA·h/g is probably due to the removal of Li from tetrahedral sites but with electrons from the Ti^{3+}/Ti^{4+} redox couple, indicating that some nontetrahedral Li cannot be removed or that some of these sites were not filled in the first place. Figure 9b ($Li_3(VAl)(PO_4)_3$) and Figure 9c ($Li_3(VCr)(PO_4)_3$) are similar. Al is inactive, and the Cr^{3+}/Cr^{4+} redox couple is high above the V^{3+}/V^{4+}one. Hence the initial parts of the charging curve are very similar to that of $Li_3V_2(PO_4)_3$. In particular, for $Li_3(VAl)(PO_4)_3$ (Figure 9b) the ordering effect around 30 mA·h/g is clearly visible. When $x = 2$ is approached in both systems (near 66 mA·h/g), Li has to be removed from the more stable tetrahedral sites, but also the V^{3+}/V^{4+} redox couple is depleted. Both these events result in a drastic increase in potential, and in practical conditions, to the end of charge. In both cases (Figure 9b,c) there is a small plateau near 4 V at the end of charge. We believe that this corresponds to the removal of Li from tetrahedral sites with the V^{3+}/V^{4+} redox couple. Perhaps some of the nontetrahedral Li cannot be removed because it is in regions with low V content. Finally, the $V_{1.5}Al_{0.5}$ compound (Figure 9d) is similar to the charging curve of the pure V materials, except that some capacity is lost from the ≈4-V plateau. This again can be understood in terms of our model. Only the V is active, so one only sees the $V^{3+/4+}$ redox couple. The step near $x = 2$ (≈60 mA·h/g) is due to accessing the tetrahedral Li. This step came at x slightly less than 2 in the other alloys but does not come early in this case since the cation dopant concentration is lower and almost all the nontetrahedral Li is accessible. The 4-V plateau becomes reduced in length by ≈50% as there is less V in the material (and hence the point where V needs to be oxidized to V^{5+} comes earlier in the charge).

In summary, we have analyzed the OCV curves of monoclinic phosphates in a systematic manner. The Li energetics and electron energies operate almost independently and the OCV curve is shaped by the sum of the two effects: Some steps are due to Li−Li interactions and Li site energetics. These are determined by the crystal structure and always occur for $x = 2.5$ and $x = 2$. Other steps are due to a change in the active redox couple. The compositions where these steps occur are due to the specific concentration of each metal. We also find that the transition metals do not interact much when mixed in the NASICON-like compounds. $Li_3(M_xN_{2-x})(PO_4)_3$ will show the features of the M and

Table 7. Voltages of Different Cation Redox Couples

redox couple	calculated voltage	experimental voltage
$Ti^{2+/3+}$	0.4	0.9[8]
$Nb^{3+/4+}$	1.1	1.8[32]
$V^{2+/3+}$	1.3	1.8[32]
$Ti^{3+/4+}$	1.6	2.5[32]
$Nb^{4+/5+}$	1.8	2.2[32]
$V^{3+/4+}$	2.5	3.8[32]
$Fe^{2+/3+}$	2.5	2.8[32]
$V^{4+/5+}$	3.3	4.6[10]
$Cr^{3+/4+}$	3.6	4.6[33]
$Mn^{3+/4+}$	3.7	inactive[34]
$Co^{3+/4+}$	4.2	4.8[33]
$Cr^{4+/5+}$	4.3	inactive[34]
$Ni^{3+/4+}$	4.3	inactive[34]
$Fe^{3+/4+}$	4.4	inactive[34]
$Fe^{4+/5+}$	4.9	inactive[34]
$Co^{4+/5+}$	5.0	inactive[34]

N redox couples separately, with little modification of one redox couple by the presence of the other metal. Given the large physical distance between the metal sites and the large "electronic separation" induced by the phosphate groups, the weak effect of alloying on the redox couple is to be expected.

Although we have focused on V (and to some extent Fe), the qualitative aspects of the features of the OCV curve should apply to other chemistries, as they arise from the geometry of the materials and the redox states of the metals. Identifying general characteristics in these materials is particularly important since many dopings and substitutions of both metal cations, intercalated cations, and anion units are possible. The features and their origins that we have identified can provide guidance for future investigations into the large class of promising Mono materials.

5.6. Voltages for Different Metal Cations. To evaluate the potential of phosphates with other transition metals, we have used first-principles methods to predict their average open circuit voltage in the monoclinic structure. The results are shown in Table 7, along with some experimental data wherever available. All calculated results were obtained with the local density approximation (LDA) except for Mn and Fe, where the generalized gradient approximation (GGA) was used. This is because high-spin Mn^{3+} and Fe^{4+} are expected to have significant Jahn−Teller effects, which are generally more accurately modeled with the GGA.[32] The calculations are average voltages over specific Li ranges: the 4+/5+ redox couples average over $x = 0 \rightarrow 1$, the 3+/4+ redox couples average over $x = 1 \rightarrow 3$, and 2+/3+ redox couples average over $x = 3 \rightarrow 3.25$. The 2+/3+ couples are less reliable than the others are because we do not know the optimal Li configuration at $x = 3.25$ and had to use intuitive considerations to estimate a location for the additional Li beyond $x = 3$. The experimental results are primarily for the rhombohedral rather than for the monoclinic structure. However, in cases where both structures have been studied very similar average voltages have been obtained (for example, the $V^{3+/4+}$ redox couple in $Li_xV_2(PO_4)_3$ is at about 3.8 V for both the Mono[10] and Rhom[8,33] structures). It should also be noted that many of the experimental redox voltages come from alloyed materials of the form $Li_xMM'(PO_4)_3$. However, it has been found that alloying has little effect on the average voltages of the redox couples (see section 5.5.2 and refs 8 and 32). For the 2+/3+ redox couple of Ti, we have used data from $Li_xFeTi(SO_4)_3$. To compare to our phosphate calculations, we shifted the voltage down by 0.8 V, consistent with what has been found for other metals when comparing phosphate and sulfate anion groups.[8,33]

The calculated voltages are uniformly too low, ranging from 0.3 to 1.3 V below the experimental values. The source of this error is not known, although the isolated metal atoms may have electron localization effects that cannot be treated very accurately with the LDA or GGA approximations. Despite significant errors, the relative voltages are qualitatively very accurate. The order of the calculated voltages matches the experiments quite closely, and almost all of the systems with the highest calculated voltages have been found to be inactive up to nearly 5 V. Therefore, although the voltage calculations do not give direct quantitative predictions, combining the experimental and computed results in Table 7 makes prediction of new material voltages possible.

6. Conclusion

We have combined computational and experimental results to understand intercalation into both rhombohedral and monoclinic structures. We have focused on the $Li_xV_2(PO_4)_3$ material but many of the results have been shown to apply to the structures in general. In the rhombohedral structure we determined that intercalation starts by filling the M1 sites with 1 Li. Then a two-phase reaction depopulates the M1 sites and fills the M3A sites. Our calculations suggest that there may be some ordering tendency at low enough temperatures.

The distinctive features in the Mono voltage curve were identified to be due to Li ordering ($x = 2.5$), Li site energetics (and Li−Li interactions) ($x = 2$), and redox couple ($x = 1$). The step due to the redox couple change will occur at different stages of the charging curve depending on the specific metal content. These underlying mechanisms largely explain the shape and features of a number of doped V compounds.

Voltage calculations were performed for a wide range of redox couples and metal cations. The results showed large quantitative errors, but careful correspondence with known experimental data shows that the qualitative ordering of the energies is accurate. As argued previously by Goodenough and co-workers,[8] the phosphate groups reduce the antibonding overlap between the oxygen and transition metal, significantly increasing the voltage. This brings many redox couples that are accessible in more close-packed oxides out of practical reach in these phosphates, and may explain why the Co, Cr, and Ni Nasicons are found to be inactive.

The simple rules we presented for the shape of the voltage curve for the monoclinic structure can be combined with the first-principles calculations of the redox voltages to predict the voltage curves for general doped $Li_3(M_xN_{2-x})(PO_4)_3$ compounds. This work demonstrates how complex materials can be analyzed, using both computational and experimental methods, obtaining insights that would be very difficult from either approach in isolation.

CM020348O

(32) Mishra, S. K.; Ceder, G. *Phys. Rev. B* **1999**, *59*, 6120.
(33) Padhi, A. K.; Nanjundaswamy, K. S.; Masquelier, C.; Okada, S.; Goodenough, J. B. *J. Electrochem. Soc.* **1997**, *144*, 1609.
(34) Saidi, Y.; Adamson, G.; Barker, J. Unpublished results obtained at Valence Technology, Henderson, NV, 2001.